Cancer Immunology, Immunotherapy (2023) 72:1285–1300
https://doi.org/10.1007/s00262-022-03334-x

RESEARCH

Oncolytic virus-mediated reducing of myeloid-derived suppressor cells enhances the efficacy of PD-L1 blockade in gemcitabine-resistant pancreatic cancer

Yoshinori Kajiwara[1] · Hiroshi Tazawa[1,2] · Motohiko Yamada[1] · Nobuhiko Kanaya[1] · Takuro Fushimi[1] · Satoru Kikuchi[1] · Shinji Kuroda[1] · Toshiaki Ohara[1,3] · Kazuhiro Noma[1] · Ryuichi Yoshida[1] · Yuzo Umeda[1] · Yasuo Urata[4] · Shunsuke Kagawa[1] · Toshiyoshi Fujiwara[1]

Received: 12 October 2022 / Accepted: 18 November 2022 / Published online: 27 November 2022

Abstract

Pancreatic ductal adenocarcinoma (PDAC) is often refractory to treatment with gemcitabine (GEM) and immune checkpoint inhibitors including anti-programmed cell death ligand 1 (PD-L1) antibody. However, the precise relationship between GEM-resistant PDAC and development of an immunosuppressive tumor microenvironment (TME) remains unclear. In this study, we investigated the immunosuppressive TME in parental and GEM-resistant PDAC tumors and assessed the therapeutic potential of combination therapy with the telomerase-specific replication-competent oncolytic adenovirus OBP-702, which induces tumor suppressor p53 protein and PD-L1 blockade against GEM-resistant PDAC tumors. Mouse PDAC cells (PAN02) and human PDAC cells (MIA PaCa-2, BxPC-3) were used to establish GEM-resistant PDAC lines. PD-L1 expression and the immunosuppressive TME were analyzed using parental and GEM-resistant PDAC cells. A cytokine array was used to investigate the underlying mechanism of immunosuppressive TME induction by GEM-resistant PAN02 cells. The GEM-resistant PAN02 tumor model was used to evaluate the antitumor effect of combination therapy with OBP-702 and PD-L1 blockade. GEM-resistant PDAC cells exhibited higher PD-L1 expression and produced higher granulocyte–macrophage colony-stimulating factor (GM-CSF) levels compared with parental cells, inducing an immunosuppressive TME and the accumulation of myeloid-derived suppressor cells (MDSCs). OBP-702 significantly inhibited GEM-resistant PAN02 tumor growth by suppressing GM-CSF-mediated MDSC accumulation. Moreover, combination treatment with OBP-702 significantly enhanced the antitumor efficacy of PD-L1 blockade against GEM-resistant PAN02 tumors. The present results suggest that combination therapy involving OBP-702 and PD-L1 blockade is a promising antitumor strategy for treating GEM-resistant PDAC with GM-CSF-induced immunosuppressive TME formation.

Keywords Pancreatic cancer · Chemoresistance · MDSC · GM-CSF · Oncolytic virus

✉ Hiroshi Tazawa
htazawa@md.okayama-u.ac.jp

[1] Department of Gastroenterological Surgery, Okayama University Graduate School of Medicine, Dentistry and Pharmaceutical Sciences, Okayama 700-8558, Japan

[2] Center for Innovative Clinical Medicine, Okayama University Hospital, 2-5-1 Shikata-cho, Kita-ku, Okayama 700-8558, Japan

[3] Department of Pathology and Experimental Medicine, Okayama University Graduate School of Medicine, Dentistry and Pharmaceutical Sciences, Okayama 700-8558, Japan

[4] Oncolys BioPharma Inc., Tokyo 105-0001, Japan

Abbreviations

BMDC	Bone marrow-derived cell
CFSE	Carboxyfluorescein diacetate succinimidyl ester
CM	Conditioned medium
CTL	Cytotoxic T lymphocyte
ELISA	Enzyme-linked immunosorbent assay
FBS	Fetal bovine serum
GAPDH	Glyceraldehyde-3-phosphate dehydrogenase
GEM	Gemcitabine
GM-CSF	Granulocyte–macrophage colony-stimulating factor
hTERT	Human telomerase reverse transcriptase
ICI	Immune checkpoint inhibitor
ICD	Immunogenic cell death

IC_{50}	50% Inhibitory concentration
MDSC	Myeloid-derived suppressor cell
MOI	Multiplicity of infection
PDAC	Pancreatic ductal adenocarcinoma
PD-L1	Programmed cell death ligand 1
PD-1	Programmed cell death 1
PFU	Plaque-forming unit
TME	Tumor microenvironment
Treg	Regulatory T cell

Introduction

Pancreatic ductal adenocarcinoma (PDAC) is a highly lethal malignancy. Total deaths due to PDAC are expected to become the second leading cause of cancer-related deaths by 2030 in the USA [1]. Despite recent advances in combination chemotherapy for the treatment of PDAC, the 5-year survival rate remains poor, at < 10% [2]. Gemcitabine (GEM) is a widely used key drug in combination chemotherapy for the treatment of locally advanced or metastatic PDAC [3]. However, the efficacy of GEM-based chemotherapy is limited in PDAC patients, and GEM resistance contributes to the poor prognosis of PDAC patients [4].

Immune checkpoint inhibitors (ICIs) targeting the programmed cell death 1 (PD-1)/programmed cell death ligand 1 (PD-L1) axis provide improved clinical outcomes in patients with several types of cancer [5]; however, the efficacy of PD-1/PD-L1 blockade is very limited against PDAC [6]. The poor response of PDAC to ICI immunotherapy is due to several immune-related factors, including low PD-L1 expression [7, 8], low tumor mutation burden [8], dense stroma [9], poor infiltration of cytotoxic T lymphocytes (CTLs) [10], and accumulation of immunosuppressive cells, such as myeloid-derived suppressor cells (MDSCs) [11], macrophages [12], and regulatory T cells (Tregs) [13]. However, the precise relationship between GEM-resistant PDAC and an immunosuppressive tumor microenvironment (TME) remains unclear.

GEM treatment is thought to induce upregulation of PD-L1 expression in PDAC cells [14] and the accumulation of MDSCs in PDAC tumors [15]. Increased PD-L1 expression on tumor cells leads to immune evasion via the induction of CTL apoptosis [16]. MDSCs are a heterogeneous population of immature myeloid cells that suppress T cell responses [17]. MDSCs infiltrate into tumors in response to a variety of inflammatory factors [17]. Thus, GEM-resistant PDAC tumors may be associated with both intrinsic and extrinsic immunosuppressive factors.

Oncolytic virotherapy is a novel antitumor treatment approach that is increasingly utilized in the treatment of PDAC [18–20]. We previously developed a telomerase-specific, replication-competent oncolytic adenovirus, OBP-301 (Suratadenoturev), in which the human telomerase reverse transcriptase (hTERT) promoter drives the expression of the viral *E1A* and *E1B* genes [21, 22]. To enhance the antitumor effect of OBP-301, we generated a modified OBP-301 variant (OBP-702) that induces expression of the tumor suppressor protein p53 by inserting the Egr1 promoter-driven p53 expression cassette into the E3 region of OBP-301 [23, 24]. We recently reported that p53-armed OBP-702 exhibits a more profound antitumor effect against human PDAC cells than non-armed OBP-301 [25]. In contrast, we also reported that OBP-502, a variant of OBP-301, facilitates the recruitment of $CD8^+$ T cells in murine PDAC tumors by inducing immunogenic cell death (ICD) [26]. However, the therapeutic potential of OBP-702 against GEM-resistant PDAC tumors in an immunosuppressive TME remains unclear.

In the present study, we investigated the relationship between GEM-resistant PDAC tumors and an immunosuppressive TME characterized by high PD-L1 expression and infiltration of immunosuppressive cells in murine PDAC tumors. The mechanism underlying development of the immunosuppressive TME induced by GEM-resistant PDAC cells was further analyzed using cytokine arrays. We then evaluated the therapeutic potential of oncolytic virotherapy with OBP-301 and OBP-702 against GEM-resistant PDAC tumors. Finally, we investigated the antitumor efficacy of combination therapy with OBP-702 and anti-PD-L1 antibody against GEM-resistant PDAC tumors.

Materials and methods

Cell lines

A mouse PDAC cell line (PAN02) derived from C57BL/6J mice was obtained from the U.S. National Cancer Institute (Frederick, MD, USA). Human PDAC cell lines (MIA PaCa-2, BxPC-3) were obtained from the American Type Culture Collection (Manassas, VA, USA). PAN02 and BxPC-3 cells were maintained in RPMI 1640 medium supplemented with 10% fetal bovine serum (FBS). MIA PaCa-2 cells were maintained in Dulbecco's Modified Eagle Medium supplemented with 10% FBS. All media were supplemented with 100 U/mL penicillin and 100 µg/mL streptomycin. The cells were routinely maintained at 37 ℃ in a humidified atmosphere with 5% CO_2. Cells were cultured for no longer than 5 months following resuscitation. The authors did not perform cell authentication analyses.

GEM-resistant PDAC cells were obtained by sequential exposure to GEM (Gemzar; Eli Lilly and Company, Indianapolis, IN, USA) over a 3-month period. The concentration of GEM was determined monthly based on the 50% inhibitory concentration (IC_{50}) values from XTT assays.

Recombinant adenoviruses

The recombinant telomerase-specific, replication-competent adenovirus OBP-301 (Suratadenoturev) drives expression of the viral *E1A* and *E1B* genes linked with an internal ribosome entry site under control of the hTERT promoter for virus replication [21, 22]. For tumor-specific induction of exogenous *p*53 expression by OBP-301, OBP-702 was constructed by inserting a human wild-type *p53* gene expression cassette derived from the Egr-1 promoter into the E3 region of OBP-301 [23, 24]. Recombinant viruses were purified by ultracentrifugation using cesium chloride step gradients. Viral titer was determined using plaque-forming assays with 293 cells, and purified virus stocks were stored at − 80 ℃.

Cell viability assay

Cells were seeded in 96-well plates at a density of 1×10^3 cells/well (PAN02, MIA PaCa-2, BxPC-3). The cells were then treated with GEM at 0, 1, 5, 10, 50, 100, 500, or 1000 nM or infected with OBP-301 or OBP-702 at a multiplicity of infection (MOI) of 0, 1, 5, 10, 50, or 100 plaque-forming units (PFUs)/cell. Cell viability was determined 3 days after treatment using a TACS® XTT Cell Proliferation Assay (R&D Systems, Minneapolis, MN, USA) according to the manufacturer's protocol.

Flow cytometric analysis

Single-cell suspensions were stained with fluorescence-conjugated antibodies. Isotype control IgG was used as a negative control. The cells were assayed for fluorescence using a BD FACSLyric™ flow cytometer (BD Biosciences, San Jose, CA, USA), and data were analyzed using FlowJo software, ver. 7.6.5. Details of antibodies used in flow cytometric analyses are shown in Table S1.

In vivo subcutaneous tumor model

Animal experimental protocols were approved by the Ethics Review Committee for Animal Experimentation of Okayama University School of Medicine (No. OKU-2018791). Parental and GEM-resistant PAN02 cells (4×10^6 cells) were subcutaneously inoculated into the flanks of 6-week-old female C57BL/6 J mice (CLEA Japan, Tokyo, Japan). Palpable tumors developed within 7 days and were permitted to grow to approximately 5–7 mm in diameter until 28 days. To evaluate the GEM sensitivity of PAN02 tumors, mice were injected intraperitoneally twice a week for 7 weeks with a 100-µL volume of solution containing GEM (100 mg/kg). To evaluate the role of GM-CSF in GEM-resistant PAN02 tumors, mice were injected subcutaneously twice a week for 28 days with a 100-µL volume of solution containing anti-GM-CSF antibody (505417; BioLegend, San Diego, CA, USA) (20 µg/mouse) or isotype IgG (400565; BioLegend) (20 µg/mouse).

To evaluate the virus sensitivity of PAN02 tumors, mice were injected intratumorally on days 0, 2, and 4 with a 50-µL volume of solution containing OBP-301 (1×10^8 PFUs) or OBP-702 (1×10^8 PFUs). To evaluate the therapeutic effect of combination therapy with OBP-702 and PD-L1 blockade, mice were injected intratumorally once a week with a 50-µL volume of solution containing OBP-702 (1×10^8 PFUs) and injected intraperitoneally twice a week for 28 days with a 100-µL volume of solution containing anti-PD-L1 antibody (200 µg/mouse). Tumor volume was calculated using the following formula: tumor volume (mm^3) $= a \times b^2 \times 0.5$, where a represents the largest diameter, b represents the smallest diameter, and 0.5 is a constant used to calculate the volume of an ellipsoid.

Histopathological analysis

Subcutaneous tumors were fixed in 10% neutralized formalin and embedded in paraffin blocks. Tissue sections (4 µm) were deparaffinized in xylene and rehydrated in a graded ethanol series. After blocking endogenous peroxidases by incubation with 3% H_2O_2 for 10 min, the samples were boiled in citrate buffer or EDTA buffer for 14 min in a microwave oven for antigen retrieval. Samples were incubated with primary antibodies for 1 h at room temperature or overnight at 4 ℃ and then with peroxidase-linked secondary antibody for 30 min at room temperature. Primary antibodies against CD8a (4SM15; eBioscience, San Diego, CA, USA), CD4 (4SM95; eBioscience), Foxp3 (FJK-16s; eBioscience), Ki67 (ab16667; Abcam, Cambridge, MA, USA), F4/80 (70076; Cell Signaling Technology, Danvers, MA, USA), CD163 (ab182422; Abcam), and arginase-1 (D4E3M; Cell Signaling Technology) were used. The enzyme substrate 3,3′-diaminobenzidine was used for visualization, and sections were counterstained with Meyer's hematoxylin. The number of cells was calculated from five randomly selected non-overlapping fields containing abundant cells. For immunofluorescence staining, primary antibody against Gr1 (RB6-8C5; eBioscience) and a fluorescence-conjugated secondary antibody were used. DAPI was used for nuclear counterstaining. Immunostained cells were photographed using a camera-equipped fluorescence microscope (IX83; Olympus, Tokyo, Japan).

Isolation of splenocytes

Tumor-bearing mice were euthanized, and spleens were surgically resected. Spleens were crushed using the blunt end of a 10-mL syringe in Petri dishes containing 10 mL of RPMI-1640 medium. The spleen mixtures were filtered

through 40-μm filters into 50-mL conical tubes and centrifuged at 400×*g* for 5 min at 4 °C. After washing with phosphate-buffered saline (PBS), cell pellets were resuspended in 5 mL of red blood cell lysis buffer (420302; BioLegend) and incubated on ice for 5 min, and the reaction was stopped by the addition of 40 mL of PBS. Single-cell suspensions were incubated with Fc Block (101320; BioLegend) for 15 min and then stained with fluorescence-conjugated antibodies and subjected to flow cytometric analysis using the antibodies listed in Table S1.

Cytokine array assay

Parental and GEM-resistant PAN02 cells were seeded in 6-well plates at a density of 1×10^5 cells/well, and the CM was collected after a 48-h incubation. A total of 40 cytokines, chemokines, and acute-phase proteins were analyzed using mouse cytokine array panel A (ARY006; R&D Systems).

Enzyme-linked immunosorbent assay (ELISA)

GM-CSF protein was quantified using a GM-CSF ELISA kit (R&D Systems) according to the manufacturer's protocol.

Quantitative real-time PCR

Total RNA was extracted from cells using a miRNeasy Mini kit (Qiagen, Valencia, CA, USA). cDNA was synthesized from 10 ng of total RNA using a TaqMan reverse transcription kit (Applied Biosystems, Foster City, CA, USA). GM-CSF and glyceraldehyde-3-phosphate dehydrogenase (GAPDH) mRNA expression was assessed using a StepOne-Plus™ real-time PCR system (Applied Biosystems) using the primers Csf2 (Mm01290062_m1) and Gapdh (Mm99999915_g1). Relative expression levels of GM-CSF mRNA were calculated according to the $2^{-\Delta\Delta Ct}$ method after normalization with reference to the expression of GAPDH mRNA.

Western blot analysis

Total protein was extracted from whole-cell lysates, and protein samples (20 μg) were electrophoresed on 8% SDS-polyacrylamide gels and transferred onto polyvinylidene difluoride transfer membranes (Hybond-P; GE Healthcare, Buckinghamshire, UK). Target proteins were detected using primary antibodies against ERK (9102; Cell Signaling Technology), phospho-ERK (9101; Cell Signaling Technology), AKT (4691; Cell Signaling Technology), phospho-Akt (4060; Cell Signaling Technology), NF-kB p65 (8242; Cell Signaling Technology), p53 (18032; Cell Signaling Technology), and β-actin mAb (A5441; Sigma-Aldrich, St. Louis, MO, USA). Horseradish peroxidase-conjugated anti-rabbit IgG (NA934; GE Healthcare) or anti-mouse IgG (NA931; GE Healthcare) were used as secondary antibodies. Immunoreactive protein bands were visualized using enhanced chemiluminescence reagent (ECL Prime; GE Healthcare).

Myeloid cell differentiation assay

Parental or GEM-resistant PAN02 cells (7×10^6 cells) seeded in T75 flasks were cultured for 48 h, and the CM was collected after centrifugation. BMDCs were obtained from the tibia and femur of 6- to 8-week-old female C57BL/6J mice and cultured in RPMI-1640 medium supplemented with 10% FBS. To investigate the differentiation of myeloid cells, BMDCs were incubated with parental or GEM-resistant PAN02 CM or culture medium containing recombinant GM-CSF (Sigma-Aldrich) (40 ng/mL). After incubation for 4 days, cells were collected, stained with fluorescence-conjugated antibodies, and assessed using flow cytometry (BD FACSLyric; BD Biosciences). Data were analyzed using FlowJo software, ver. 7.6.5. Details of antibodies are shown in Table S1.

Statistical analyses

Statistical analyses were performed using JMP software, version 14.3.0, and GraphPad Prism 8 software was used to create graphics. Variance between groups was compared. The Student's *t* test was used to compare differences in means between two groups, and analysis of variance with Tukey's test was used to compare differences in means between multiple groups. Data are presented as mean ± SD. *P* values < 0.05 were considered statistically significant.

Results

GEM-resistant PDAC cells exhibit high PD-L1 expression

To investigate the relationship between GEM resistance and immunosuppressive potential in PDAC cells, we established a mouse GEM-resistant PDAC cell line, PAN02, and two human GEM-resistant PDAC cell lines (MIA PaCa-2 and BxPC-3) by sequential exposure to GEM, with the concentration determined monthly over a 3-month period based on XTT assay IC_{50} values (Fig. 1A). After establishment of GEM-resistant PDAC cells, we compared the GEM sensitivity between parental and GEM-resistant cells using the XTT assay (Fig. 1B). The GEM IC_{50} values of GEM-resistant PDAC cells were more than threefold higher than those of the parental cells. We then investigated the expression level of PD-L1 on the surface of parental and GEM-resistant

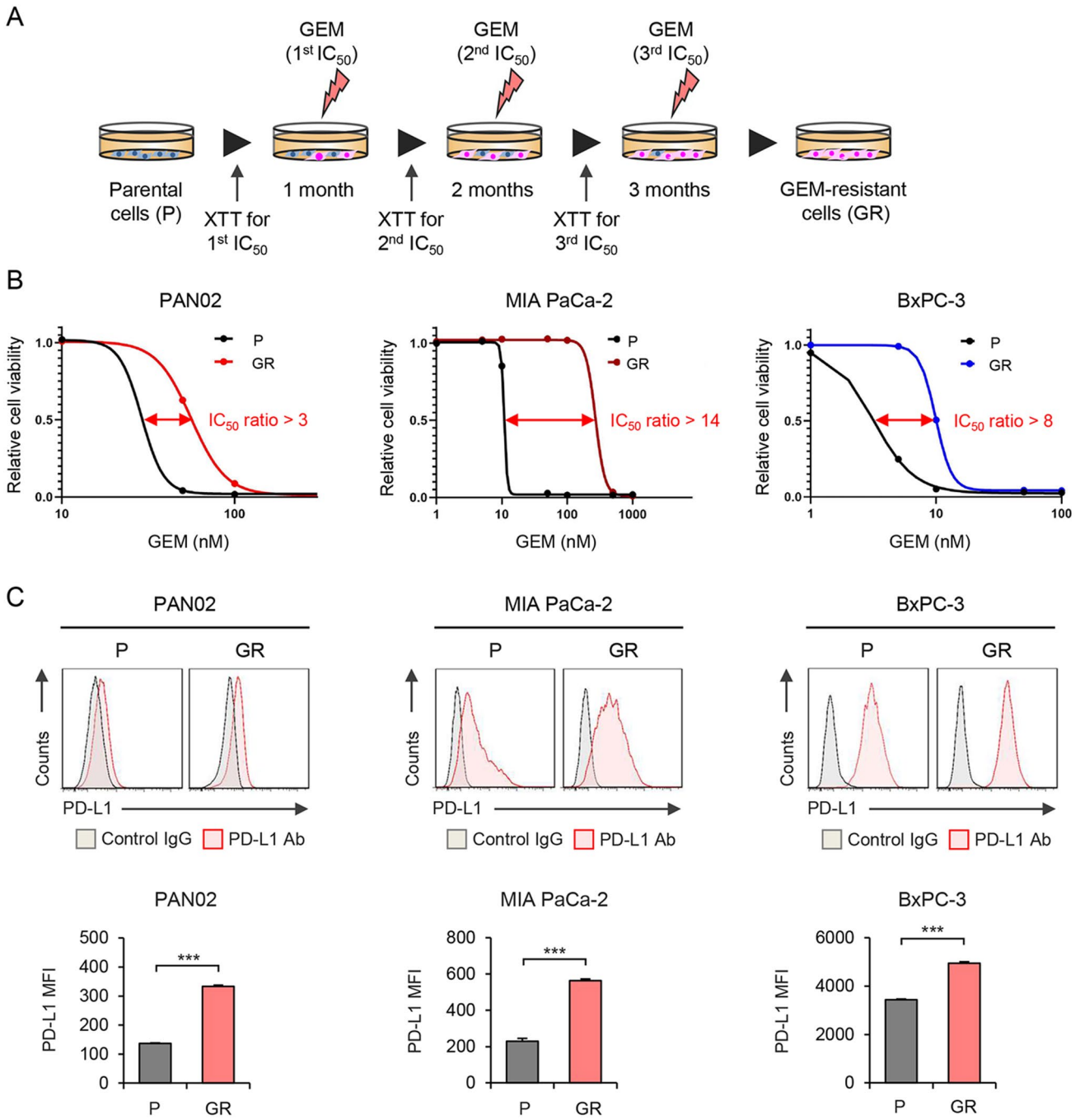

Fig. 1 Establishment of GEM-resistant PDAC cells and analysis of PD-L1 expression in parental and GEM-resistant PDAC cells. **A** Schematic illustration of gemcitabine (GEM) treatment protocol. Parental (P) PDAC cells (PAN02, MIA PaCa-2, BxPC-3) were treated with GEM for 3 months to obtain GEM-resistant (GR) PDAC cells. **B** Parental and GR PDAC cells were treated with GEM at the indicated doses for 6 days. Cell viability was quantified using the XTT assay and calculated relative to that of P cells, which was set at 1.0. The ratio of 50% inhibitory concentration (IC_{50}) between P and GR PDAC cells is shown. **C** Expression of PD-L1 in P and GR PDAC cells was assessed using flow cytometric analysis. The mean fluorescence intensity (MFI) of PD-L1 expression for each cell line was determined by calculating the difference between the MFI of anti-PD-L1 antibody-treated and control IgG-treated cells. Data are expressed as mean ± SD ($n = 3$ in each group; $^*P < 0.05$)

PDAC cells using flow cytometry (Fig. 1C). GEM-resistant PDAC cells expressed significantly higher levels of PD-L1 protein compared with parental cells. These results suggest that GEM-resistant PDAC cells express high levels of PD-L1.

To investigate the relationship between GEM resistance and PD-L1 expression in PDAC tumors, we developed

subcutaneous parental and GEM-resistant PAN02 tumor models using immunocompetent mice. Parental and GEM-resistant PAN02 cells were inoculated into syngeneic mice subcutaneously, and the mice were treated with intraperitoneal administration of GEM (100 mg/kg) twice a week for 7 weeks (Figure S1A). GEM treatment similarly inhibited the growth of both parental and GEM-resistant PAN02 tumors until day 14. However, by day 49, the growth of GEM-resistant PAN02 tumors was significantly greater than that of the parental tumors (Figure S1B), and the weight of GEM-resistant PAN02 tumors was significantly greater than that of the parental tumors (Figure S1C). Western blot analysis of tumor proteins demonstrated that GEM-resistant PAN02 tumors expressed higher levels of PD-L1 than the parental tumors (Figure S1D). These results suggest that GEM-resistant PDAC cells develop GEM-resistant tumors that express high levels of PD-L1.

GEM-resistant PAN02 tumors induce an immunosuppressive TME with MDSC accumulation

To investigate whether GEM-resistant PDAC tumors induce an immunosuppressive TME, parental and GEM-resistant PAN02 tumors were analyzed by immunohistochemistry (Fig. 2A). The number of $CD8^+$ T cells was lower and the number of $CD4^+$ T cells higher in GEM-resistant PAN02 tumors compared with the parental tumors, although the differences were not significant. GEM-resistant PAN02 tumors exhibited a significantly higher proportion of $Gr1^+$ myeloid cells, arginase-1^+ MDSCs, and $Foxp3^+$ Treg cells than parental tumors. However, the proportion of $F4/80^+$ macrophages was significantly lower in GEM-resistant PAN02 tumors than parental tumors, and the proportion of $CD163^+$ M2 macrophages was similar between the tumors. In contrast, the number of $Ki67^+$ proliferating tumor cells was significantly lower in GEM-resistant PAN02 tumors compared with parental tumors. These results suggest that GEM-resistant PAN02 tumors induce the accumulation of immunosuppressive MDSCs and Treg cells.

To investigate whether GEM-resistant PDAC tumors systemically induce an immunosuppressive TME in mice, we analyzed the proportion of immune cells in the spleens of mice without and with parental and GEM-resistant PAN02 tumors by flow cytometry (Fig. 2B). The proportion of $CD8^+$ T cells was significantly lower in the spleens of GEM-resistant PAN02 tumor-bearing mice compared with control or parental tumor-bearing mice. GEM-resistant PAN02 tumor-bearing mice exhibited a significantly higher percentage of $CD4^+$ T cells compared with control mice. However, there was no increase in the proportion of $CD4^+Foxp3^+$ Treg cells in the spleens of GEM-resistant PAN02 tumor-bearing mice (Figure S1E). In contrast, GEM-resistant PAN02 tumor-bearing mice exhibited a significantly higher proportion of $CD11b^+$ myeloid cells and $CD11b^+Gr1^+$ MDSCs in the spleen compared with control or parental tumor-bearing mice. These results suggest that GEM-resistant PDAC tumors systemically induce the accumulation of MDSCs in the spleen.

GEM-resistant PAN02 cells promote an increase in the proportion of MDSCs via GM-CSF production

To explore the underlying mechanism of systemic MDSC accumulation induced by GEM-resistant PDAC cells in mice, a cytokine array was used to identify the cytokines/chemokines produced by GEM-resistant PAN02 cells (Figure S2). Among 40 cytokines/chemokines examined, the levels of 14 cytokines were higher and 26 cytokines lower in GEM-resistant PAN02 conditioned medium (CM) compared with parental CM. As granulocyte–macrophage colony-stimulating factor (GM-CSF) is reportedly associated with MDSC accumulation in PDAC tumors [27, 28], we further analyzed the amount of GM-CSF in parental and GEM-resistant PAN02 CM by ELISA (Fig. 3A). GEM-resistant PAN02 CM contained 400-fold more GM-CSF than parental CM. RT-PCR analysis demonstrated that the expression level of GM-CSF mRNA was 60-fold higher in GEM-resistant PAN02 cells than parental cells (Fig. 3B). These results suggest that GM-CSF released by GEM-resistant PDAC cells is a potent inducer of MDSC accumulation.

To investigate whether GEM-resistant PDAC cell-derived GM-CSF induces the differentiation of MDSCs, we used flow cytometry to analyze the proportion of MDSCs in Bone marrow-derived cells (BMDCs) incubated with parental CM, GEM-resistant PAN02 CM, or recombinant GM-CSF (Figure S3). Both GEM-resistant PAN02 CM and GM-CSF significantly increased the proportion of $CD11b^+Gr1^+$ MDSCs compared with parental CM. In terms of MDSC phenotype, the proportion of $CD11b^+Ly6G^+$ granulocytic MDSCs was significantly increased following incubation with GEM-resistant PAN02 CM compared with parental CM. In contrast, treatment with anti-GM-CSF antibody significantly reduced the proportion of $CD11b^+Gr1^+$ MDSCs induced by GEM-resistant PAN02 CM (Fig. 3C). These results suggest that GEM-resistant PAN02 cells induce MDSC differentiation via GM-CSF production.

GEM-resistant PAN02 cells and GM-CSF enhance the immunosuppressive potential of MDSCs

To evaluate the activity of MDSCs induced by GEM-resistant PAN02 cells, MDSC proliferation was analyzed by flow cytometry using cells labeled with carboxyfluorescein diacetate succinimidyl ester (CFSE), the level of which gradually decreases as MDSCs proliferate (Figure

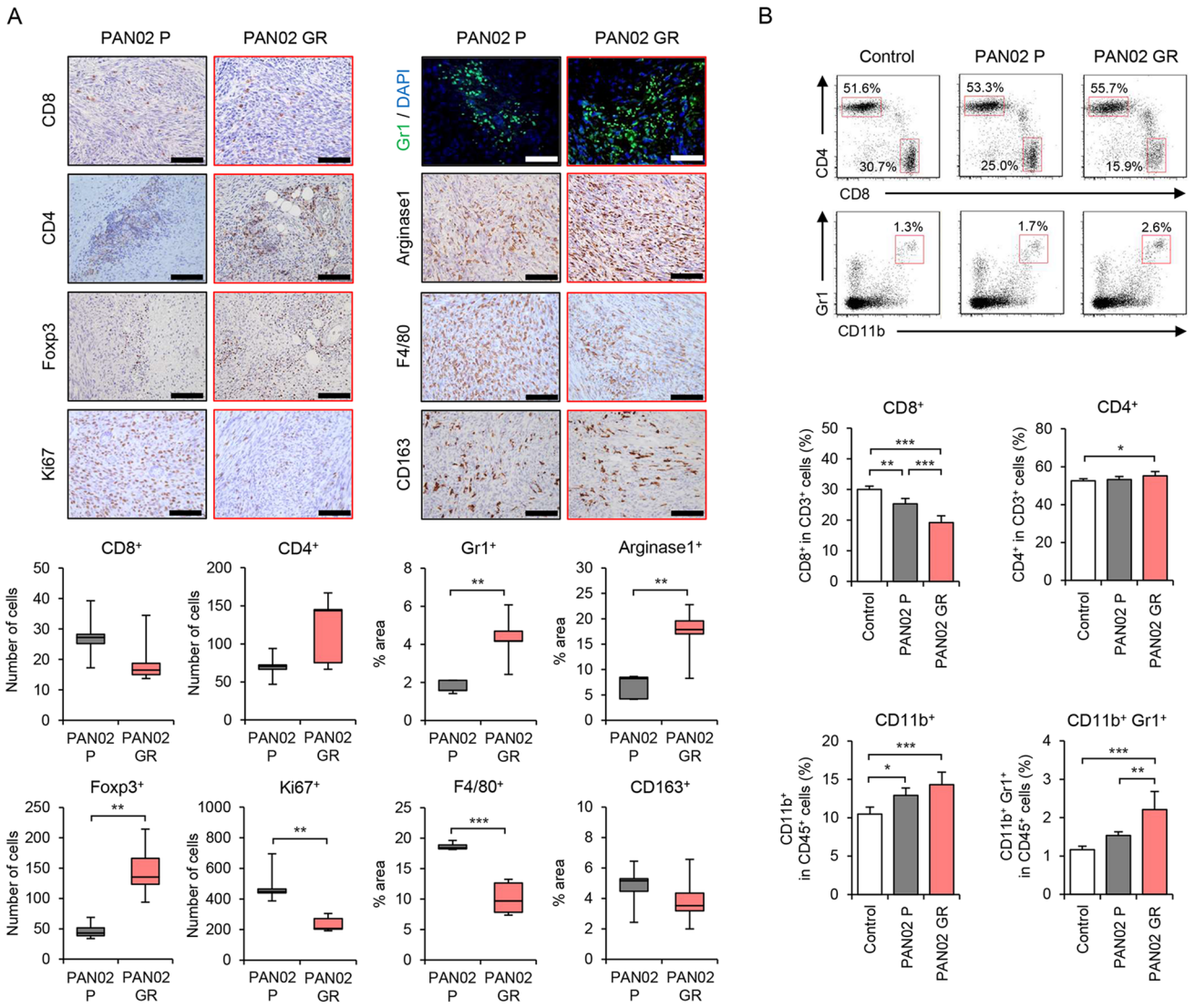

Fig. 2 Immunohistochemical staining and flow cytometric analysis of P and GR PAN02 tumors and spleens. **A** Representative photographs of immunohistochemical staining for $CD8^+$ T cells, $CD4^+$ T cells, $Foxp3^+$ Tregs, $Ki67^+$ cells, $Gr1^+$ MDSCs, arginase-1^+ MDSCs, $F4/80^+$ macrophages, and $CD163^+$ M2 macrophages in each group. Scale bars, 100 μm. The number of $CD8^+$ T cells, $CD4^+$ T cells, Foxp3 + Tregs, and $Ki67^+$ cells and the percent area of $Gr1^+$ MDSCs, arginase-1^+ MDSCs, $F4/80^+$ macrophages, $CD163^+$ M2 macrophages was calculated from five different randomly selected fields. **B** Representative data of flow cytometric analysis of CD8, CD4, CD11b, and Gr1 in each group. The percentages of $CD8^+$ T cells and $CD4^+$ T cells among $CD3^+$ cells and the percentages of $CD11b^+$ myeloid cells and $CD11b^+Gr1^+$ MDSCs among $CD45^+$ cells are shown. Data are expressed as mean ± SD ($n = 5$ in each group; $^*P < 0.05$; $^{**}P < 0.01$; $^{***}P < 0.001$)

S4A). Compared with parental CM, both GEM-resistant PAN02 CM and GM-CSF significantly increased MDSC proliferation, determined as the percentage of the CFSE-low population. Moreover, we used flow cytometry to analyze the level of PD-L1 expression on the surface of MDSCs incubated with parental or GEM-resistant PDAC CM (Figure S4B). Both GEM-resistant PAN02 CM and GM-CSF, but not parental CM, significantly increased the PD-$L1^+$ population among $CD11b^+Gr1^+$ MDSCs. To evaluate the immunosuppressive activity of MDSCs, we analyzed the proliferation of $CD8^+$ T cells co-cultured with MDSCs induced by parental and GEM-resistant PAN02 CM or GM-CSF (Figure S4C). The proliferation of $CD8^+$ T cells was significantly reduced in the presence of MDSCs induced by GEM-resistant PAN02 CM or GM-CSF compared with $CD8^+$ T cells in the presence of MDSCs induced by parental CM. These results suggest that GEM-resistant PDAC cells enhance the immunosuppressive activity of MDSCs.

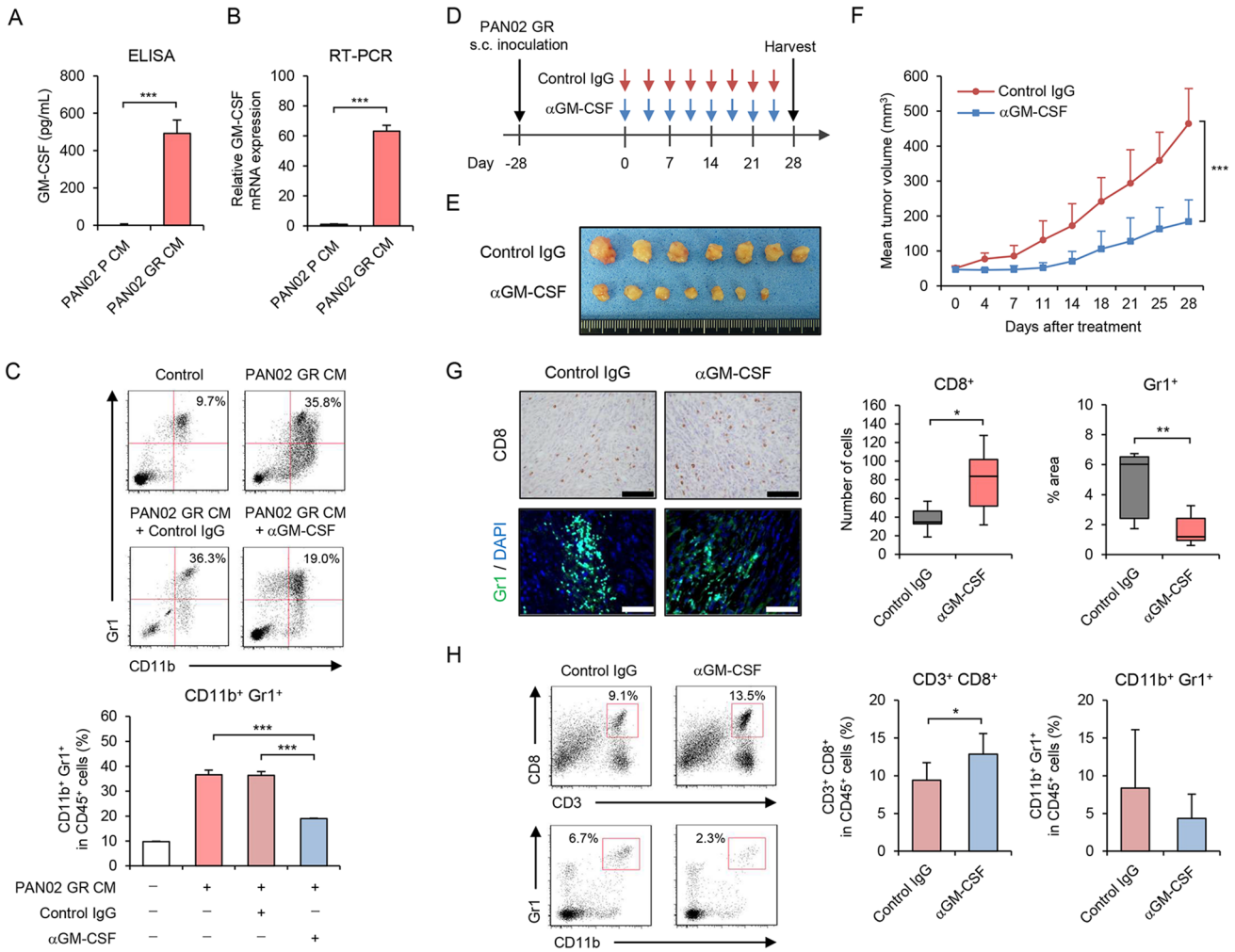

Fig. 3 Anti-GM-CSF antibody treatment suppresses tumor growth and immunosuppressive TME induced by GR PAN02 cells. **A** Conditioned medium (CM) of P and GR PAN02 cells was used to analyze the amount of extracellular GM-CSF using ELISA. **B** Expression of GM-CSF mRNA was analyzed using quantitative RT-PCR. GM-CSF mRNA expression of GR PAN02 cells was calculated relative to that of P cells, which was set at 1.0. **C** Representative data of flow cytometric analysis for CD11b and Gr1 in each group. The percentage of $CD11b^+Gr1^+$ MDSCs among $CD45^+$ cells is shown. Data are expressed as mean ± SD ($n = 3$ in each group). **D** GR PAN02 cells (4×10^6 cells/site) were inoculated into the flanks of C57BL/6J mice on day − 28. Anti-GM-CSF antibody (red arrows) or control isotype IgG (blues arrows) was intraperitoneally administered twice a week for four cycles. **E** Photographs of tumors in control isotype IgG and anti-GM-CSF antibody groups. **F** Tumor growth curves of control IgG- and anti-GM-CSF antibody-treated PAN02 tumors. **G** Representative photographs of immunohistochemical staining for $CD8^+$ T cells or $Gr1^+$ MDSCs in each group. Scale bars, 100 μm. The number of $CD8^+$ T cells and percent area of $Gr1^+$ MDSCs were calculated from five different randomly selected fields. **H** Representative data of flow cytometric analysis of CD3, CD8, CD11b, and Gr1 in each group. The percentages of $CD3^+CD8^+$ T cells and $CD11b^+Gr1^+$ MDSCs among $CD45^+$ cells are shown. Data are expressed as mean ± SD ($n = 7$ in each group; $^*P < 0.05$; $^{**}P < 0.01$; $^{***}P < 0.001$)

GM-CSF blockade inhibits GEM-resistant PAN02 tumor growth and MDSC accumulation

To evaluate the role of GM-CSF in inducing an immunosuppressive TME in GEM-resistant PAN02 tumors, we treated GEM-resistant PAN02 tumor models with anti-GM-CSF antibody or control IgG (Fig. 3D). Intratumoral injection of anti-GM-CSF antibody significantly suppressed the growth of GEM-resistant PAN02 tumors compared with control IgG treatment (Fig. 3E, F). Neither GM-CSF nor anti-GM-CSF antibody affected the proliferation of GEM-resistant PAN02 cells (Figure S5), suggesting GM-CSF blockade exerts an indirect antitumor effect, probably via the induction of an antitumor immune response. Immunohistochemical analysis of tumors demonstrated that anti-GM-CSF antibody treatment significantly increased the number of $CD8^+$ T cells and decreased the number of $Gr1^+$ MDSCs compared with control IgG treatment (Fig. 3G). Flow cytometric analysis demonstrated that anti-GM-CSF antibody treatment significantly increased the proportion of $CD3^+CD8^+$ T cells in the

spleen, whereas there was a moderate decrease in the number of $CD11b^+Gr1^+$ MDSCs (Fig. 3H). These results suggest that GM-CSF is a key regulator of MDSC accumulation in GEM-resistant PAN02 tumors.

OBP-702 inhibits GEM-resistant PAN02 cell viability and GM-CSF production by suppressing multiple signaling pathways

We recently demonstrated that the telomerase-specific oncolytic adenoviruses OBP-301 and OBP-702 exhibit antitumor activity against human and murine PDAC cells [25, 26]. To evaluate the therapeutic potential of these viruses against GEM-resistant PDAC tumors, we first analyzed the in vitro antitumor effect of OBP-301 and OBP-702 against parental and GEM-resistant PAN02 cells using the XTT assay (Fig. 4A). OBP-702 exhibited a more profound antitumor effect than OBP-301 against parental and GEM-resistant PAN02 cells. These results suggest that OBP-702 is more effective than OBP-301 against GEM-resistant PAN02 cells.

To determine whether the oncolytic adenoviruses suppress GM-CSF production in GEM-resistant PAN02 cells, the amount of GM-CSF in CM of GEM-resistant PAN02 cells infected with OBP-702 or OBP-301 was analyzed by ELISA (Fig. 4B). Both OBP-702 and OBP-301 significantly decreased the production of GM-CSF in GEM-resistant PAN02 cells, but the effect of OBP-702 was more potent than that of OBP-301. RT-PCR analysis revealed that both OBP-702 and OBP-301 significantly decreased the expression of GM-CSF mRNA in GEM-resistant PAN02 cells (Fig. 4C). These results suggest that OBP-702 reduces GM-CSF production in GEM-resistant PDAC cells.

GM-CSF production is regulated by several signaling pathways, including the KRAS/ERK [28], PI3K/AKT [28], and NF-kB pathways [29]. To monitor the activation of these signaling pathways and the inhibitory effect of the oncolytic adenoviruses in GEM-resistant PAN02 cells, we used Western blotting to analyze ERK, AKT, and NF-kB protein levels in parental and GEM-resistant PAN02 cells and virus-infected GEM-resistant PAN02 cells. The levels of phosphorylated ERK, phosphorylated AKT, and NF-kB were increased in GEM-resistant PAN02 cells compared with parental cells (Fig. 4D). OBP-702 reduced the levels of phosphorylated ERK, phosphorylated AKT, and NF-kB in GEM-resistant PAN02 cells more strongly than OBP-301 (Fig. 4E). These results suggest that OBP-702 reduces GM-CSF production in GEM-resistant PDAC cells by downregulating the ERK/AKT/NF-kB signaling pathways.

OBP-702 indirectly reduces the immunosuppressive potential of MDSCs

To determine whether OBP-702 suppresses the immunosuppressive activity of MDSCs, we examined the differentiation, proliferation, and PD-L1 expression of MDSCs and proliferation of $CD8^+$ T cells using flow cytometry. The proportion of MDSCs increased following incubation of BMDCs with GEM-resistant PAN02 CM for 4 days. OBP-702 significantly suppressed the differentiation of $CD11b^+Gr1^+$ MDSCs from BMDCs (Fig. 4F). The proportion of $CD11b^+Ly6G^+$ granulocytic MDSCs declined significantly following OBP-702 treatment (Figure S6A). OBP-702 also significantly reduced the proliferation of MDSCs induced by GEM-resistant PAN02 CM (Figure S6B). Moreover, OBP-702 significantly decreased the proportion of $PD\text{-}L1^+$ MDSCs (Fig. 4G). In contrast, the proliferation of $CD8^+$ T cells increased significantly following OBP-702 treatment during co-culture with MDSCs induced by GEM-resistant PAN02 CM (Figure S6C). To exclude the possibility of a direct cytopathic effect of the oncolytic adenoviruses against immune cells, we investigated the therapeutic effect of OBP-301 and OBP-702 against BMDCs and MDSCs using the XTT assay. Neither OBP-301 nor OBP-702 affected the viability of BMDCs or $CD11b^+Gr1^+$ MDSCs (Figure S7). These results suggest that OBP-702 inhibits the immunosuppressive activity of MDSCs.

OBP-702 inhibits GEM-resistant PAN02 tumor growth and MDSC accumulation

To evaluate the therapeutic potential of the oncolytic adenoviruses against GEM-resistant PDAC tumors, we analyzed the in vivo antitumor effects of OBP-301 and OBP-702 using GEM-resistant PAN02 tumor models. Mice bearing GEM-resistant PAN02 tumors were injected intratumorally with either OBP-301 or OBP-702 every other day for a total of 3 injections (Fig. 5A). Both OBP-301 and OBP-702 significantly suppressed the growth of GEM-resistant PAN02 tumors compared with the control (Fig. 5B, C and Figure S8A). The mean tumor weight was significantly lower in virus-treated mice than control mice (Figure S8B). Neither the control nor virus-treated mice exhibited any weight loss during the experiment (Figure S8C). These results suggest that OBP-301 and OBP-702 are effective against GEM-resistant PAN02 tumors.

To determine whether the oncolytic adenoviruses affect the immunosuppressive TME in GEM-resistant PDAC tumors, GEM-resistant PAN02 tumors and spleens of mice treated with OBP-301 or OBP-702 were analyzed using immunohistochemistry and flow cytometry, respectively. Immunohistochemical analysis of the tumors demonstrated that OBP-301 and OBP-702 significantly increased the

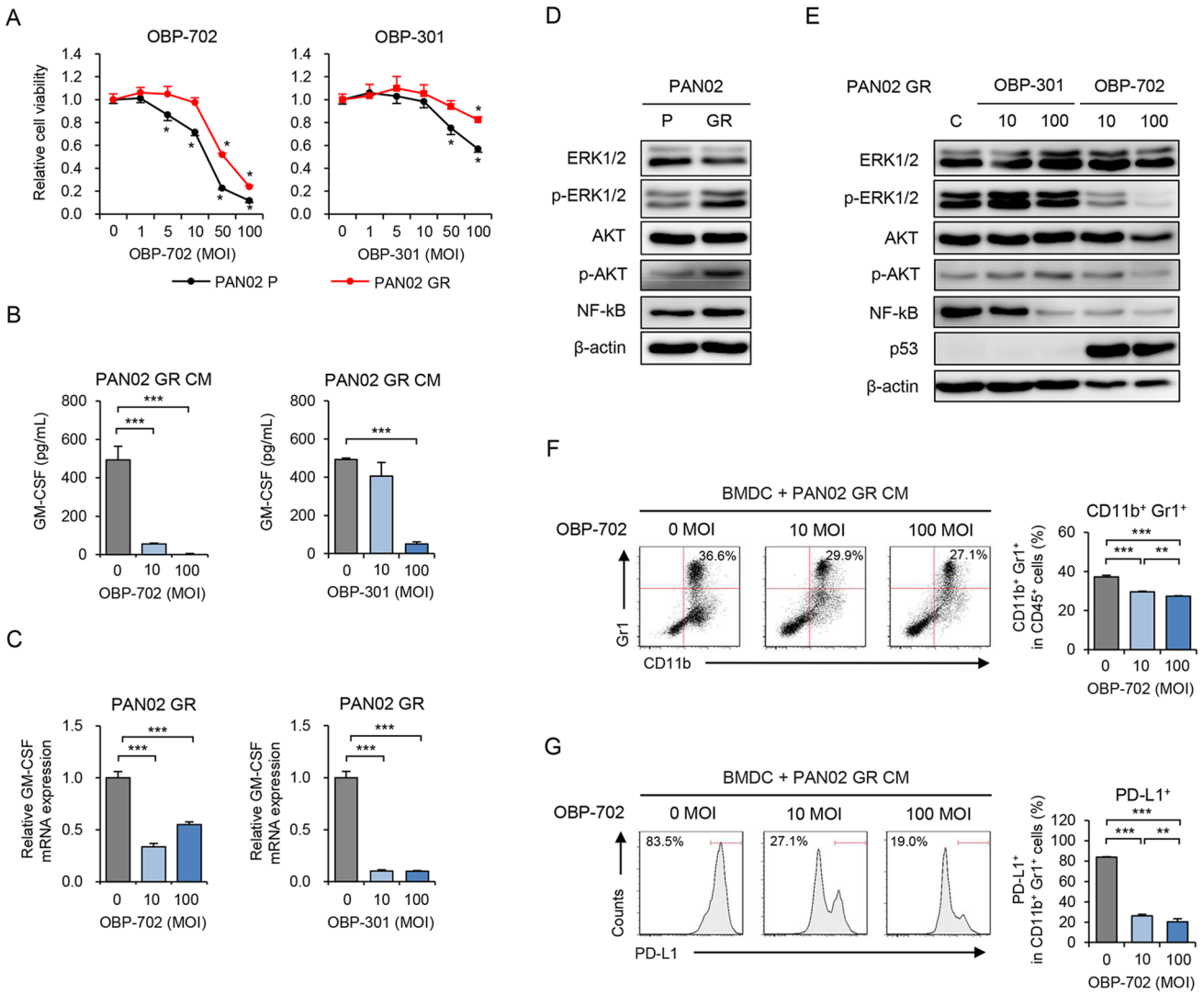

Fig. 4 OBP-702 suppresses GM-CSF production, oncogenic signals, and MDSC differentiation induced by GR PDAC cells. **A** P and GR PAN02 cells were treated with OBP-301 or OBP-702 at the indicated MOIs for 72 h. Cell viability was quantified using the XTT assay. Cell viability was calculated relative to that of the mock-infected group, which was set at 1.0. Cell viability data are expressed as mean ± SD ($n = 5$ in each group). **B** CM of GR PAN02 cells treated with OBP-702 or OBP-301 at the indicated MOIs for 72 h was used to analyze the amount of extracellular GM-CSF using ELISA. **C** Expression of GM-CSF mRNA in GR PAN02 cells treated with OBP-702 or OBP-301 at the indicated MOIs for 72 h was analyzed using quantitative RT-PCR. GM-CSF mRNA expression of GR PAN02 cells was calculated relative to that of P cells, which was set at 1.0. **D** Cell lysates of P and GR PAN02 cells were subjected to Western blot analysis of ERK1/2, phosphorylated ERK1/2, AKT, phosphorylated AKT, and NF-kB. β-Actin was assayed as a loading control. **E** GR PAN02 cells were infected with OBP-301 or OBP-702 at the indicated MOIs for 72 h. Cell lysates were subjected to Western blot analysis of ERK1/2, phosphorylated ERK1/2, AKT, phosphorylated AKT, NF-kB, and p53. β-Actin was assayed as a loading control. **F** Representative data of flow cytometric analysis of CD11b and Gr1 in each group. The percentage of $CD11b^+Gr1^+$ MDSCs among $CD45^+$ cells is shown for BMDCs incubated with GR PAN02 CM and OBP-702 at the indicated MOIs. **G** Representative data of flow cytometric analysis of PD-L1 in each group. The percentage of $PD\text{-}L1^+$ cells among $CD11b^+Gr1^+$ MDSCs is shown for BMDCs incubated with GR PAN02 CM and OBP-702 at the indicated MOIs. Data are expressed as mean ± SD ($n = 3$ in each group; $^*P < 0.05$; $^{**}P < 0.01$; $^{***}P < 0.001$)

number of $CD8^+$ T cells, and the effect of OBP-702 was significantly stronger than that of OBP-301 (Fig. 5D). The percent area of $Gr1^+$ MDSCs was significantly lower in virus-treated tumors compared with control tumors, with OBP-301 and OBP-702 exhibiting a similar effect (Fig. 5D). In contrast, the results of flow cytometry demonstrated that OBP-702, but not OBP-301, significantly increased the percentage of $CD8^+$ T cells and decreased the percentage of $CD11b^+Gr1^+$ MDSCs in the spleen (Fig. 5E). These results suggest that OBP-702 is superior to OBP-301 in reducing

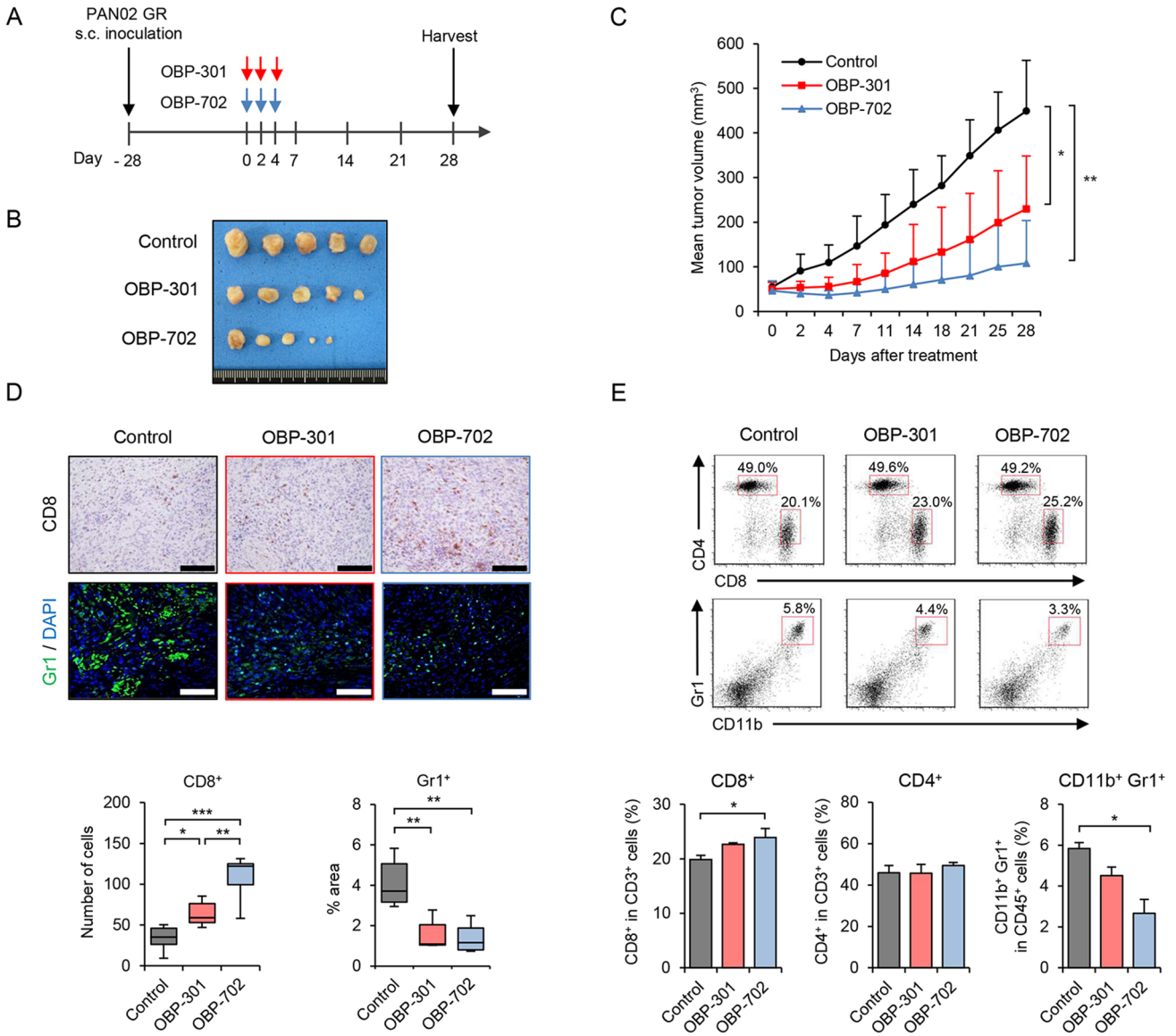

Fig. 5 In vivo antitumor effects of OBP-702 and OBP-301 against GR PAN02 tumors. **A** GR PAN02 cells (4×10^6 cells/site) were inoculated into the flanks of C57BL/6J mice on day − 28. OBP-301 (red arrows) or OBP-702 (blue arrows) was injected intratumorally at 1×10^8 PFUs on days 0, 2, and 4. One experiment has been performed. **B** Photographs of tumors in the control, OBP-301, and OBP-702 groups. **C** Tumor growth curves for non-treated control (black line), OBP-301-treated (red line), and OBP-702-treated (blue line) mice. **D** Representative photographs of immunohistochemical staining of $CD8^+$ T cells and $Gr1^+$ MDSCs in each group. Scale bars, 100 μm. The number of $CD8^+$ T cells and percent area of $Gr1^+$ MDSCs were calculated from five different randomly selected fields. **E** Representative data of flow cytometric analysis of CD8, CD4, CD11b, and Gr1 in each group. The percentages of $CD8^+$ T cells and $CD4^+$ T cells among $CD3^+$ cells and the percentage of $CD11b^+Gr1^+$ MDSCs among $CD45^+$ cells are shown. Data are expressed as mean ± SD ($n=7$ in each group; $^*P<0.05$; $^{**}P<0.01$; $^{***}P<0.001$)

tumor growth and the development of an immunosuppressive TME in GEM-resistant PDAC tumors.

Combination immunotherapy with OBP-702 and PD-L1 blockade

Finally, to determine whether OBP-702 enhances the antitumor efficacy of anti-PD-L1 antibody treatment against GEM-resistant PDAC tumors, GEM-resistant PAN02 tumor-bearing mice were treated with anti-PD-L1 antibody, OBP-702, or combination therapy (Fig. 6A). Compared with the control, combination therapy more significantly suppressed the growth of GEM-resistant PAN02 tumors than anti-PD-L1 antibody or OBP-702 monotherapy (Fig. 6B, C and Figure S9A). The mean tumor weight of mice treated with combination therapy was significantly lower than that of

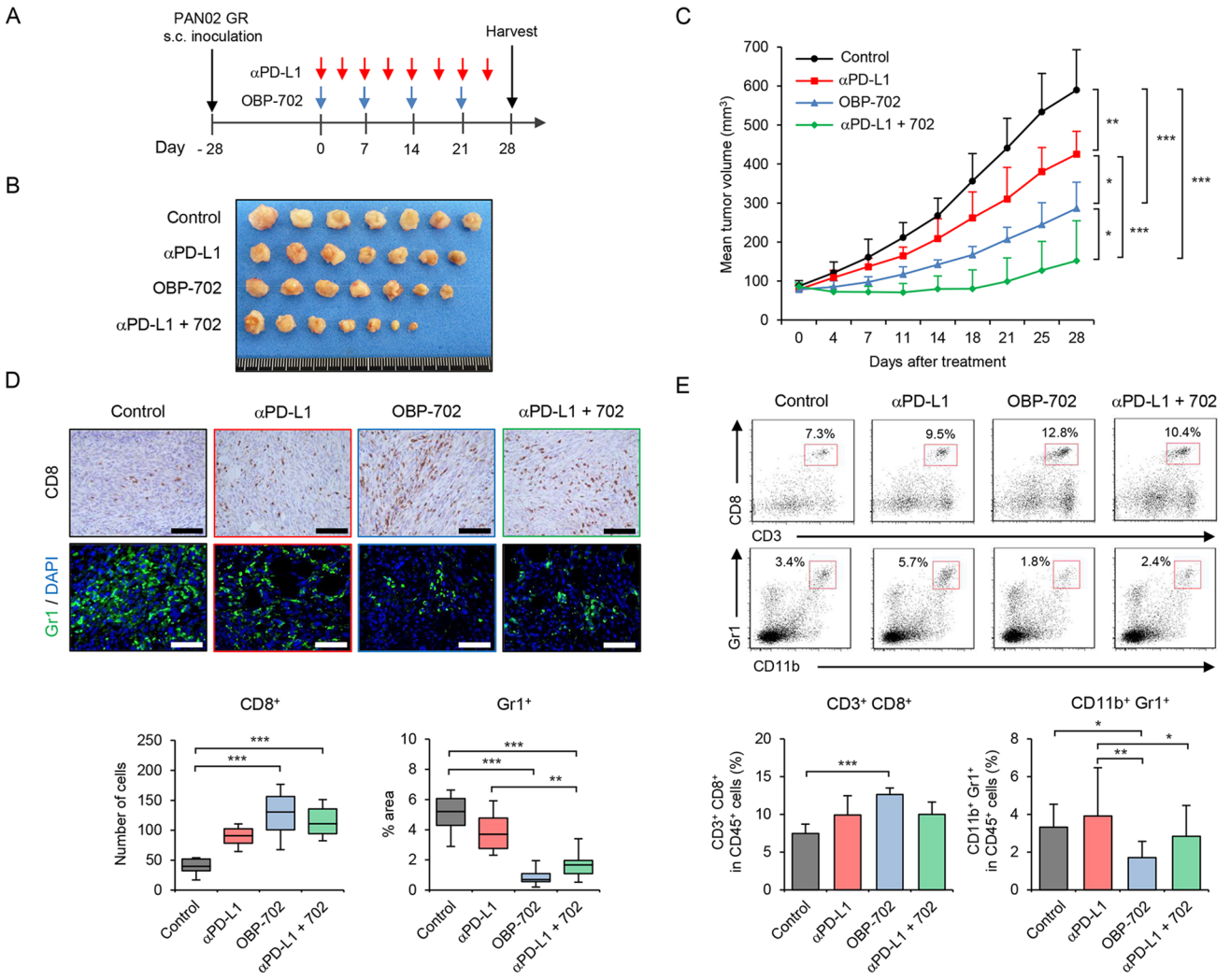

Fig. 6 In vivo antitumor effects of OBP-702 and anti-PD-L1 antibody against GR PAN02 tumors. **A** GR PAN02 cells (4×10^6 cells/site) were inoculated into the flanks of C57BL/6 J mice on day − 28. Anti-PD-L1 antibody was intraperitoneally administered twice a week for four cycles (red arrows). OBP-702 (blue arrows) was injected intratumorally at 1×10^8 PFUs every week for four cycles. One experiment has been performed. **B** Photographs of tumors in the control, anti-PD-L1 antibody-treated, OBP-702-treated, and combination treatment groups. **C** Tumor growth curves for non-treated control (black line), anti-PD-L1 antibody-treated (red line), OBP-702-treated (blue line), and combination treatment (green line) mice. **D** Representative photographs of immunohistochemical staining of $CD8^+$ T cells and $Gr1^+$ MDSCs in each group. Scale bars, 100 μm. The number of $CD8^+$ T cells and the percent area of $Gr1^+$ MDSCs were calculated from five different randomly selected fields. **E** Representative data of flow cytometric analysis of CD3, CD8, CD11b, and Gr1 in each group. The percentages of $CD3^+CD8^+$ T cells and $CD11b^+Gr1^+$ MDSCs among $CD45^+$ cells are shown. Data are expressed as mean ± SD ($n=7$ in each group; $^*P<0.05$; $^{**}P<0.01$; $^{***}P<0.001$)

monotherapy-treated and control mice (Figure S9B). Neither the control nor treated mice exhibited any weight loss during the experiment (Figure S9C). These results suggest that combination therapy with oncolytic adenovirus is more effective against GEM-resistant PAN02 tumors than PD-L1 blockade monotherapy.

To determine whether combination therapy affects development of the immunosuppressive TME in GEM-resistant PDAC tumors, GEM-resistant PAN02 tumors and spleens of mice treated with combination therapy or monotherapy were analyzed using immunohistochemistry and flow cytometry, respectively. Immunohistochemical staining of tumors demonstrated that both combination therapy and OBP-702 monotherapy significantly increased the number of tumor-infiltrating $CD8^+$ T cells compared with control tumors (Fig. 6D). The percent area of $Gr1^+$ MDSCs was significantly lower in GEM-resistant PAN02 tumors of mice treated with combination therapy or OBP-702 monotherapy compared with the control (Fig. 6D). Flow cytometry analysis demonstrated that OBP-702 monotherapy significantly increased the percentage of $CD3^+CD8^+$ T cells and decreased the percentage of $CD11b^+Gr1^+$ MDSCs in

the spleen (Fig. 6E). These results suggest that combination therapy with OBP-702 and anti-PD-L1 antibody is a promising treatment option for GEM-resistant PDAC tumors exhibiting MDSC accumulation.

Discussion

The therapeutic efficacy of GEM against PDAC is limited by the acquisition of GEM resistance by tumor cells [4]. Although developments in immunotherapy with ICIs have brought new hope to certain cancer patients [5], the clinical benefits of ICIs are not sufficient in PDAC patients due to a poor antitumor immune response [6]. In this study, we demonstrated that GEM-resistant PDAC cells exhibit high PD-L1 expression and promote an immunosuppressive TME with MDSC accumulation via GM-CSF production. The telomerase-specific replication-competent oncolytic adenovirus OBP-702 exhibited good therapeutic potential by directly inducing cytopathic effects and indirectly reducing the immunosuppressive TME in GEM-resistant PDAC tumors via suppression of GM-CSF production. Moreover, combination therapy involving PD-L1 blockade and OBP-702 exhibited a more profound antitumor effect against GEM-resistant PDAC tumors than PD-L1 blockade alone. These findings indicate that use of OBP-702 to improve the antitumor efficacy of ICIs against GEM-resistant PDAC with an immunosuppressive TME represents a potent therapeutic strategy.

GEM-resistant PDAC cells exhibited higher PD-L1 expression than parental cells (Fig. 1), suggesting that PD-L1 plays a role in the chemoresistance of PDAC. High PD-L1 expression is associated with poor prognosis in PDAC patients [30, 31]. Doi et al. demonstrated that activation of several oncogenic signaling pathways, including JAK/STAT, ERK/MAPK, AKT, and NF-kB, is involved in GEM-mediated PD-L1 upregulation in PDAC cells [14]. A relationship between PD-L1 activation and the DNA damage repair pathway has also been suggested [32]. Inhibition of PD-L1 by certain small synthetic peptides increases apoptosis of human PDAC cells [33]. Although the precise role of PD-L1 in GEM-resistant PDAC remains unclear, targeting PD-L1 expression may reverse both immunosuppression and chemoresistance in PDAC.

The accumulation of myeloid cells such as MDSCs and macrophages is thought to play a central role in the immunosuppressive TME of PDAC [34]. Previous reports have shown that GEM treatment inhibits the accumulation of MDSCs in PAN02 tumors [35, 36]. In contrast, GEM treatment in human PDAC cells increases the secretion of inflammatory cytokines to enhance the differentiation of monocytes into MDSCs [15]. Then, we hypothesized that GEM treatment induces more immunosuppressive TME in GEM-resistant PAN02 tumors compared to parental tumors. To evaluate the immunosuppressive TME induced by GEM-resistant PAN02 cells, we compared parental and GEM-resistant PAN02 tumors after treatment with GEM for 7 weeks (Figure S1). In the present study, the immunosuppressive TME of GEM-resistant PAN02 tumors was characterized by increased infiltration of MDSCs rather than macrophages (Fig. 2), suggesting MDSCs play a critical role in GEM-resistant PDAC. In a genetically engineered mouse model of PDAC, targeted depletion of MDSCs enhanced the T cell immune response and subsequent tumor cell apoptosis [11]. Moreover, there are some reports to support the critical role of MDSCs in a mouse PAN02 tumor model. Treatment with zoledronic acid reduces the accumulation MDSCs, resulting in the suppression of tumor growth [37]. The histone deacetylase inhibitor entinostat was shown to significantly suppress the accumulation of MDSCs, thereby improving the antitumor efficacy of ICI immunotherapy [38]. Thus, GEM-resistant PDAC-driven MDSC accumulation represents a druggable target to improve the outcome of patients with PDAC that is refractory to GEM-based chemotherapy.

The present study identified GM-CSF as a potent inflammatory mediator that induces MDSC accumulation in GEM-resistant PAN02 tumors. The inflammatory role of GM-CSF was confirmed by the decrease in MDSC accumulation and increase in the T cell immune response in GEM-resistant PAN02 tumors following treatment with anti-GM-CSF antibody (Fig. 3). High GM-CSF expression is associated with poor prognosis in PDAC patients [15]. Accumulating evidence indicates that GEM treatment increases GM-CSF production in PDAC and breast cancer cells via activation of the ERK/AKT/NF-kB signaling pathways in both in vitro and in vivo settings [15, 39]. In addition, MDSC accumulation in the TME is regulated not only by tumor cells but also cancer-associated stromal cells [17, 40]. Pancreatic satellite cells are reportedly involved in MDSC accumulation in PDAC [41]. We recently demonstrated that OBP-702-mediated p53 induction in cancer-associated fibroblasts suppresses the peritoneal metastasis of human gastric cancer cells by reducing the secretion of cancer-promoting cytokines [42], suggesting the potential role of OBP-702 in the stromal TME. Therefore, exploration of the underlying mechanism of GM-CSF-mediated MDSC accumulation could facilitate the development of novel antitumor modalities for the treatment of GEM-resistant PDAC.

It is worth noting that GEM-resistant PAN02 tumors showed a significantly higher proportion of immunosuppressive Foxp3$^+$ Treg cells as well as MDSCs compared with parental tumors (Fig. 2). On the underlying mechanism of Treg cell accumulation, a cytokine array demonstrated that GEM-resistant PAN02 cells produced higher amount of CCL5 compared to parental cells (Figure

S2), suggesting the possible involvement of CCL5 in the accumulation of Treg cells. Tan et al. demonstrated that knockdown of CCL5 in tumor cells or treatment with CCL5 receptor inhibitor suppressed the growth of PAN02 tumors by reducing the accumulation of Treg cells [43]. Wang et al. also showed the therapeutic potential of anti-CCL5 antibody to suppress the growth of PAN02 tumors in monotherapy [44] and combination therapy with PD-L1 blockade [45] by reducing the accumulation of Treg cells. Although the underlying mechanism of Treg cell accumulation in GEM-resistant PAN02 tumors remains unclear, CCL5 production by GEM-resistant tumor cells may be involved in the development of immunosuppressive TME with accumulation of Treg cells.

Oncolytic virotherapy is a novel antitumor treatment approach that is increasingly utilized in the treatment of PDAC [18–20]. OBP-702 exhibited a profound antitumor effect in GEM-resistant PDAC tumors in the present study, and this effect was mediated by suppression of GM-CSF production via downregulation of the ERK, AKT, and NF-kB signaling pathways (Figs. 4, 5). GM-CSF plays dual immunostimulatory and immunosuppressive roles [46]. Serafini et al. suggested that treatment with high doses of a vaccine that stimulates GM-CSF production induces development of an immunosuppressive TME rather than immunostimulatory TME via the accumulation of MDSCs [47]. Indeed, the antitumor efficacy against PDAC of the GM-CSF-expressing vaccine GVAX [48] and GM-CSF-expressing oncolytic herpes simplex virus T-vec [20] was shown to be insufficient when combined with chemotherapy and ICIs. Given the immunosuppressive role of GM-CSF in GEM-resistant PDAC, GM-CSF suppression may be more effective than GM-CSF-inducing immunotherapy for treating GEM-resistant PDAC tumors with high GM-CSF production.

Combination immunotherapy involving ICIs and oncolytic virotherapy is considered a promising strategy for treating PDAC with an immunosuppressive TME [49]. In this study, combination treatment with OBP-702 significantly enhanced the antitumor efficacy of PD-L1 blockade in GEM-resistant PAN02 tumors by suppressing GM-CSF-mediated MDSC accumulation and enhancing the T cell immune response (Fig. 6). Chemoradiotherapy enhances the antitumor efficacy of PD-L1 blockade against PAN02 tumors by inducing ICD-mediated T cell immune responses [30, 50]. However, GEM-resistant PDAC tumors are resistant to conventional therapy. We recently reported that OBP-702 exerts profound antitumor activity against chemoresistant osteosarcoma cells [51]. OBP-301 sensitizes human lung cancer cells to GEM treatment via modulation of cell cycle [52]. Although whether OBP-702 sensitizes GEM-resistant PDAC cells to GEM treatment remains to be elucidated, OBP-702 may be a potent therapeutic option for improving the antitumor efficacy of GEM and ICIs against GEM-resistant PDAC tumors by modulating the chemosensitivity and immunosuppressive TME.

In conclusion, we demonstrated that GEM-resistant PDAC tumors induce the development of an immunosuppressive TME with GM-CSF-mediated accumulation of MDSCs. We also demonstrated that combination treatment with the telomerase-specific oncolytic adenovirus OBP-702 enhances the efficacy of PD-L1 blockade against GEM-resistant PDAC tumors by suppressing the GM-CSF-mediated development of an immunosuppressive TME. Combination therapy with OBP-702 and PD-L1 blockade is thus an effective strategy for treating GEM-resistant PDAC tumors. Taken together, our data indicate that oncolytic virus-mediated modulation of the immunosuppressive TME is a novel therapeutic option for use in combination with immunotherapy in the treatment of GEM-resistant PDAC.

Supplementary Information The online version contains supplementary material available at https://doi.org/10.1007/s00262-022-03334-x.

Acknowledgements We thank Tomoko Sueishi, Yuko Hoshijima, and Tae Yamanishi for their excellent technical support.

Author contributions Conception and design: HT, SKa, TFuj; development of methodology: YK, MY, NK, TFus; acquisition of data: YK, MY, TFus; analysis and interpretation of data: YK, MY, TFus; writing, review, and/or revision of the manuscript: YK, HT, TFuj; administrative, technical, or material support: YU; study supervision: HT, SKi, SKu, TO, KN, RY, YU, SKa, TFuj

Funding This study was supported in part by grants from the Japan Agency for Medical Research and Development (17ck0106285h0001 and 20ck0106569h0001 to T. Fujiwara) and JSPS KAKENHI grants JP16K10596 and JP21K07219 to H. Tazawa and JP16H05416 and JP19H03731 to T. Fujiwara.

Declarations

Competing interests Y. Urata is President & CEO of Oncolys BioPharma Inc. H. Tazawa and T. Fujiwara are consultants of Oncolys BioPharma Inc. The other authors have no potential conflicts of interest to disclose.

Conflict of interest Y. Urata is President & CEO of Oncolys BioPharma Inc. H. Tazawa and T. Fujiwara are consultants of Oncolys BioPharma Inc. The other authors have no potential conflicts of interest to disclose.

References

1. Rahib L, Smith BD, Aizenberg R, Rosenzweig AB, Fleshman JM, Matrisian LM (2014) Projecting cancer incidence and deaths to 2030: the unexpected burden of thyroid, liver, and pancreas cancers in the United States. Cancer Res 74:2913–2921. https://doi.org/10.1158/0008-5472.CAN-14-0155
2. Siegel RL, Miller KD, Fuchs HE, Jemal A (2021) Cancer Statistics, 2021. CA Cancer J Clin 71:7–33. https://doi.org/10.3322/caac.21654

3. Burris HA 3rd, Moore MJ, Andersen J et al (1997) Improvements in survival and clinical benefit with gemcitabine as first-line therapy for patients with advanced pancreas cancer: a randomized trial. J Clin Oncol 15:2403–2413. https://doi.org/10.1200/JCO.1997.15.6.2403
4. Gu Z, Du Y, Zhao X, Wang C (2021) Tumor microenvironment and metabolic remodeling in gemcitabine-based chemoresistance of pancreatic cancer. Cancer Lett 521:98–108. https://doi.org/10.1016/j.canlet.2021.08.029
5. Sun C, Mezzadra R, Schumacher TN (2018) Regulation and function of the PD-L1 checkpoint. Immunity 48:434–452. https://doi.org/10.1016/j.immuni.2018.03.014
6. Leinwand J, Miller G (2020) Regulation and modulation of antitumor immunity in pancreatic cancer. Nat Immunol 21:1152–1159. https://doi.org/10.1038/s41590-020-0761-y
7. Herbst RS, Soria JC, Kowanetz M et al (2014) Predictive correlates of response to the anti-PD-L1 antibody MPDL3280A in cancer patients. Nature 515:563–567. https://doi.org/10.1038/nature14011
8. Yarchoan M, Albacker LA, Hopkins AC et al (2019) PD-L1 expression and tumor mutational burden are independent biomarkers in most cancers. JCI Insight 4:e126908. https://doi.org/10.1172/jci.insight.126908
9. Gorchs L, Kaipe H (2021) Interactions between cancer-associated fibroblasts and T cells in the pancreatic tumor microenvironment and the role of chemokines. Cancers (Basel) 13:2995. https://doi.org/10.3390/cancers13122995
10. Blando J, Sharma A, Higa MG et al (2019) Comparison of immune infiltrates in melanoma and pancreatic cancer highlights VISTA as a potential target in pancreatic cancer. Proc Natl Acad Sci USA 116:1692–1697. https://doi.org/10.1073/pnas.1811067116
11. Stromnes IM, Brockenbrough JS, Izeradjene K, Carlson MA, Cuevas C, Simmons RM, Greenberg PD, Hingorani SR (2014) Targeted depletion of an MDSC subset unmasks pancreatic ductal adenocarcinoma to adaptive immunity. Gut 63:1769–1781. https://doi.org/10.1136/gutjnl-2013-306271
12. Candido JB, Morton JP, Bailey P et al (2018) CSF1R(+) macrophages sustain pancreatic tumor growth through T cell suppression and maintenance of key gene programs that define the squamous subtype. Cell Rep 23:1448–1460. https://doi.org/10.1016/j.celrep.2018.03.131
13. Viehl CT, Moore TT, Liyanage UK, Frey DM, Ehlers JP, Eberlein TJ, Goedegebuure PS, Linehan DC (2006) Depletion of CD4+CD25+ regulatory T cells promotes a tumor-specific immune response in pancreas cancer-bearing mice. Ann Surg Oncol 13:1252–1258. https://doi.org/10.1245/s10434-006-9015-y
14. Doi T, Ishikawa T, Okayama T et al (2017) The JAK/STAT pathway is involved in the upregulation of PD-L1 expression in pancreatic cancer cell lines. Oncol Rep 37:545–554. https://doi.org/10.3892/or.2017.5399
15. Takeuchi S, Baghdadi M, Tsuchikawa T et al (2015) Chemotherapy-derived inflammatory responses accelerate the formation of immunosuppressive myeloid cells in the tissue microenvironment of human pancreatic cancer. Cancer Res 75:2629–2640. https://doi.org/10.1158/0008-5472.CAN-14-2921
16. Dong H, Strome SE, Salomao DR et al (2002) Tumor-associated B7–H1 promotes T-cell apoptosis: a potential mechanism of immune evasion. Nat Med 8:793–800. https://doi.org/10.1038/nm730
17. Gabrilovich DI, Nagaraj S (2009) Myeloid-derived suppressor cells as regulators of the immune system. Nat Rev Immunol 9:162–174. https://doi.org/10.1038/nri2506
18. Ady JW, Heffner J, Klein E, Fong Y (2014) Oncolytic viral therapy for pancreatic cancer: current research and future directions. Oncolytic Virother 3:35–46. https://doi.org/10.2147/OV.S53858
19. Nattress CB, Hallden G (2018) Advances in oncolytic adenovirus therapy for pancreatic cancer. Cancer Lett 434:56–69. https://doi.org/10.1016/j.canlet.2018.07.006
20. Haller SD, Monaco ML, Essani K (2020) The present status of immuno-oncolytic viruses in the treatment of pancreatic cancer. Viruses 12:1318. https://doi.org/10.3390/v12111318
21. Kawashima T, Kagawa S, Kobayashi N et al (2004) Telomerase-specific replication-selective virotherapy for human cancer. Clin Cancer Res 10:285–292. https://doi.org/10.1158/1078-0432.ccr-1075-3
22. Hashimoto Y, Watanabe Y, Shirakiya Y et al (2008) Establishment of biological and pharmacokinetic assays of telomerase-specific replication-selective adenovirus. Cancer Sci 99:385–390. https://doi.org/10.1111/j.1349-7006.2007.00665.x
23. Yamasaki Y, Tazawa H, Hashimoto Y et al (2012) A novel apoptotic mechanism of genetically engineered adenovirus-mediated tumour-specific p53 overexpression through E1A-dependent p21 and MDM2 suppression. Eur J Cancer 48:2282–2291. https://doi.org/10.1016/j.ejca.2011.12.020
24. Hasei J, Sasaki T, Tazawa H et al (2013) Dual programmed cell death pathways induced by p53 transactivation overcome resistance to oncolytic adenovirus in human osteosarcoma cells. Mol Cancer Ther 12:314–325. https://doi.org/10.1158/1535-7163.MCT-12-0869
25. Koujima T, Tazawa H, Ieda T et al (2020) Oncolytic virus-mediated targeting of the ERK signaling pathway inhibits invasive propensity in human pancreatic cancer. Mol Ther Oncolytics 17:107–117. https://doi.org/10.1016/j.omto.2020.03.016
26. Kanaya N, Kuroda S, Kakiuchi Y et al (2020) Immune modulation by telomerase-specific oncolytic adenovirus synergistically enhances antitumor efficacy with Anti-PD1 antibody. Mol Ther 28:794–804. https://doi.org/10.1016/j.ymthe.2020.01.003
27. Bayne LJ, Beatty GL, Jhala N, Clark CE, Rhim AD, Stanger BZ, Vonderheide RH (2012) Tumor-derived granulocyte-macrophage colony-stimulating factor regulates myeloid inflammation and T cell immunity in pancreatic cancer. Cancer Cell 21:822–835. https://doi.org/10.1016/j.ccr.2012.04.025
28. Pylayeva-Gupta Y, Lee KE, Hajdu CH, Miller G, Bar-Sagi D (2012) Oncogenic Kras-induced GM-CSF production promotes the development of pancreatic neoplasia. Cancer Cell 21:836–847. https://doi.org/10.1016/j.ccr.2012.04.024
29. Schreck R, Baeuerle PA (1990) NF-kappa B as inducible transcriptional activator of the granulocyte-macrophage colony-stimulating factor gene. Mol Cell Biol 10:1281–1286. https://doi.org/10.1128/mcb.10.3.1281-1286.1990
30. Nomi T, Sho M, Akahori T et al (2007) Clinical significance and therapeutic potential of the programmed death-1 ligand/programmed death-1 pathway in human pancreatic cancer. Clin Cancer Res 13:2151–2157. https://doi.org/10.1158/1078-0432.CCR-06-2746
31. Danilova L, Ho WJ, Zhu Q et al (2019) Programmed cell death ligand-1 (PD-L1) and CD8 expression profiling identify an immunologic subtype of pancreatic ductal adenocarcinomas with favorable survival. Cancer Immunol Res 7:886–895. https://doi.org/10.1158/2326-6066.CIR-18-0822
32. Sato H, Jeggo PA, Shibata A (2019) Regulation of programmed death-ligand 1 expression in response to DNA damage in cancer cells: Implications for precision medicine. Cancer Sci 110:3415–3423. https://doi.org/10.1111/cas.14197
33. Wang F, Ma J, Liu J, Jin H, Huang D (2012) Synthetic small peptides acting on B7H1 enhance apoptosis in pancreatic cancer cells. Mol Med Rep 6:553–557. https://doi.org/10.3892/mmr.2012.970
34. Vonderheide RH, Bear AS (2020) Tumor-derived myeloid cell chemoattractants and T cell exclusion in pancreatic cancer. Front Immunol 11:605619. https://doi.org/10.3389/fimmu.2020.605619

35. Ghansah T, Vohra N, Kinney K, Weber A, Kodumudi K, Springett G, Sarnaik AA, Pilon-Thomas S (2013) Dendritic cell immunotherapy combined with gemcitabine chemotherapy enhances survival in a murine model of pancreatic carcinoma. Cancer Immunol Immunother 62:1083–1091. https://doi.org/10.1007/s00262-013-1407-9
36. Eriksson E, Wenthe J, Irenaeus S, Loskog A, Ullenhag G (2016) Gemcitabine reduces MDSCs, tregs and TGFbeta-1 while restoring the teff/treg ratio in patients with pancreatic cancer. J Transl Med 14:282. https://doi.org/10.1186/s12967-016-1037-z
37. Porembka MR, Mitchem JB, Belt BA, Hsieh CS, Lee HM, Herndon J, Gillanders WE, Linehan DC, Goedegebuure P (2012) Pancreatic adenocarcinoma induces bone marrow mobilization of myeloid-derived suppressor cells which promote primary tumor growth. Cancer Immunol Immunother 61:1373–1385. https://doi.org/10.1007/s00262-011-1178-0
38. Christmas BJ, Rafie CI, Hopkins AC et al (2018) Entinostat converts immune-resistant breast and pancreatic cancers into checkpoint-responsive tumors by reprogramming tumor-infiltrating MDSCs. Cancer Immunol Res 6:1561–1577. https://doi.org/10.1158/2326-6066.CIR-18-0070
39. Wu C, Tan X, Hu X, Zhou M, Yan J, Ding C (2020) Tumor microenvironment following gemcitabine treatment favors differentiation of immunosuppressive Ly6C(high) myeloid cells. J Immunol 204:212–223. https://doi.org/10.4049/jimmunol.1900930
40. Fultang N, Li X, Li T, Chen YH (2020) Myeloid-derived suppressor cell differentiation in cancer: transcriptional regulators and enhanceosome-mediated mechanisms. Front Immunol 11:619253. https://doi.org/10.3389/fimmu.2020.619253
41. Mace TA, Ameen Z, Collins A et al (2013) Pancreatic cancer-associated stellate cells promote differentiation of myeloid-derived suppressor cells in a STAT3-dependent manner. Cancer Res 73:3007–3018. https://doi.org/10.1158/0008-5472.CAN-12-4601
42. Ogawa T, Kikuchi S, Tabuchi M et al (2022) Modulation of p53 expression in cancer-associated fibroblasts prevents peritoneal metastasis of gastric cancer. Mol Ther Oncolytics 25:249–261. https://doi.org/10.1016/j.omto.2022.04.009
43. Tan MC, Goedegebuure PS, Belt BA, Flaherty B, Sankpal N, Gillanders WE, Eberlein TJ, Hsieh CS, Linehan DC (2009) Disruption of CCR5-dependent homing of regulatory T cells inhibits tumor growth in a murine model of pancreatic cancer. J Immunol 182:1746–1755. https://doi.org/10.4049/jimmunol.182.3.1746
44. Wang X, Lang M, Zhao T et al (2017) Cancer-FOXP3 directly activated CCL5 to recruit FOXP3(+)Treg cells in pancreatic ductal adenocarcinoma. Oncogene 36:3048–3058. https://doi.org/10.1038/onc.2016.458
45. Wang X, Li X, Wei X et al (2020) PD-L1 is a direct target of cancer-FOXP3 in pancreatic ductal adenocarcinoma (PDAC), and combined immunotherapy with antibodies against PD-L1 and CCL5 is effective in the treatment of PDAC. Signal Transduct Target Ther 5:38. https://doi.org/10.1038/s41392-020-0144-8
46. Bhattacharya P, Budnick I, Singh M, Thiruppathi M, Alharshawi K, Elshabrawy H, Holterman MJ, Prabhakar BS (2015) Dual role of GM-CSF as a pro-inflammatory and a regulatory cytokine: implications for immune therapy. J Interferon Cytokine Res 35:585–599. https://doi.org/10.1089/jir.2014.0149
47. Serafini P, Carbley R, Noonan KA, Tan G, Bronte V, Borrello I (2004) High-dose granulocyte-macrophage colony-stimulating factor-producing vaccines impair the immune response through the recruitment of myeloid suppressor cells. Cancer Res 64:6337–6343. https://doi.org/10.1158/0008-5472.CAN-04-0757
48. Tsujikawa T, Crocenzi T, Durham JN et al (2020) Evaluation of cyclophosphamide/gvax pancreas followed by Listeria–Mesothelin (CRS-207) with or without Nivolumab in patients with pancreatic cancer. Clin Cancer Res 26:3578–3588. https://doi.org/10.1158/1078-0432.CCR-19-3978
49. Jiang J, Zhou H, Ni C, Hu X, Mou Y, Huang D, Yang L (2019) Immunotherapy in pancreatic cancer: new hope or mission impossible? Cancer Lett 445:57–64. https://doi.org/10.1016/j.canlet.2018.10.045
50. Azad A, Yin Lim S, D'Costa Z, et al (2017) PD-L1 blockade enhances response of pancreatic ductal adenocarcinoma to radiotherapy. EMBO Mol Med 9:167–180. https://doi.org/10.15252/emmm.201606674
51. Sugiu K, Tazawa H, Hasei J et al (2021) Oncolytic virotherapy reverses chemoresistance in osteosarcoma by suppressing MDR1 expression. Cancer Chemother Pharmacol 88:513–524. https://doi.org/10.1007/s00280-021-04310-5
52. Liu D, Kojima T, Ouchi M, Kuroda S, Watanabe Y, Hashimoto Y, Onimatsu H, Urata Y, Fujiwara T (2009) Preclinical evaluation of synergistic effect of telomerase-specific oncolytic virotherapy and gemcitabine for human lung cancer. Mol Cancer Ther 8:980–987. https://doi.org/10.1158/1535-7163.MCT-08-0901